FLORE
Repository istituzionale dell'Università degli Studi di Firenze

Deciphering past and present atmospheric metal pollution of urban environments: The role of black crusts formed on historical

(Article begins on next page)

10 August 2024

Deciphering past and present atmospheric metal pollution of urban environments: the role of black crusts formed on historical constructions

Cristina García-Florentino[1], Maite Maguregui[2,*], Chiara Ciantelli[3], Alessandro Sardella[3], Alessandra Bonazza[3], Ignasi Queralt[4], Jose Antonio Carrero[1], Claudio Natali[5], Héctor Morillas[1,6], Juan Manuel Madariaga[1], Gorka Arana[1]

[1] Department of Analytical Chemistry, Faculty of Science and Technology, University of the Basque Country UPV/EHU, P.O. Box 644, 48080 Bilbao, Basque Country, Spain

[2] Department of Analytical Chemistry, Faculty of Pharmacy, University of the Basque Country UPV/EHU, P.O. Box 450, 01080 Vitoria-Gasteiz, Basque Country, Spain

[3] Institute of Atmospheric Sciences and Climate, National Research Council (ISAC-CNR), Via Piero Gobetti, 101, 40129, Bologna, Italy

[4] Department of Geosciences, IDAEA-CSIC, Jordi Girona 18-26, 08034 Barcelona, Spain

[5] Department of Earth Sciences, University of Florence, Florence, Italy

[6] Department of Mathematics and Experimental Sciences Didactics, Faculty of Education, Philosophy and Anthropology, University of the Basque Country UPV/EHU, II Building, Oñati Plaza 3, 20018 Donostia-San Sebastian, Basque Country, Spain

*Corresponding author. E-mail: maite.maguregui@ehu.eus

ABSTRACT

Construction materials affected by black crusts (BCs) can be subjected to restoration, demolition, recycling or even to their management as waste products, thus determining their chemical features should be considered a crucial step before to undertake any action. In this work, we present the development of an analytical methodology useful to be implemented as a routine screening tool to detect recent and past atmospheric emissions of heavy metals, nowadays superficially deposited or even encapsulated in BCs. For its development, BCs together with their corresponding construction materials were sampled from the historical construction Punta Begoña Galleries (Getxo, Basque Country, North of Spain). To detect the superficial (recent depositions) and internal (past accumulations) metallic accumulations in the BCs quickly and in a cost-effective way, BCs thin sections were analysed by elemental spectroscopic imaging techniques (SEM-EDS and μ-ED-XRF). Additionally, Raman imaging studies allowed to perform the molecular speciation study of lead, the main metal accumulated inner in the BCs and coming from past atmospheric deposition events. To propose the reactivity pathway, which leads to the formation of the lead compounds, chemical equilibrium modelling was used. Finally, ICP-MS technique allowed determining the concentration of main metals accumulated in the total mass of the BCs, and through lead isotopic ratio analysis the possible source of metallic particles emission was also approached.

1. INTRODUCTION

Buildings located in city centres are directly exposed to high concentrations of atmospheric pollutants. In this sense, the monitoring of pollutants and their deposition are crucial to check the environmental health and also to identify guidelines in Cultural Heritage preservation. In the past, the attention of researchers was focused mainly on the role of gaseous pollutants on stone or mortar deteriorations, especially on sulphur dioxide [1]. However, in many cities of Europe, the levels of SO_2 have been reduced while the huge increase in automobile traffic has promoted a considerable rise in the levels of ozone, nitrogen oxides and Total Suspended Particulate Matter [1,2], being aerosol derived from combustion processes the main cause of atmospheric pollution in urban environments after gaseous contamination [3]. This fact has generated a new air pollution scenario [1].

Atmospheric pollutants (gaseous and particulate) can be deposited and accumulated in construction materials. Moreover, construction materials can also incorporate pollutants through a capillary migration promoted after a direct contact of the building material with contaminated waters or soil coming from industrial processes (mining, steel work, tannery, chrome plating or galvanic process, etc.). Sometimes it is not necessary a direct contact with the contamination source, since a lixiviation processes can also promote the migration of pollutants to the construction materials.

In previous works, it was demonstrated that black crusts (BCs) formed on construction materials have the ability to trap volatile organic compounds (e.g. aliphatic hydrocarbons, carboxylic acids, etc. [4] polycyclic aromatic hydrocarbons (PAHs) [5], and metallic particles [6]. These characteristic black patinas are usually formed due to the interaction of the calcium carbonate present on the material and the atmospheric SO_2 following a dry or wet deposition (incorporation in the rainwater) of this acid gaseous pollutant. As a result of the H_2SO_4 reaction with calcium carbonate, sulphates (mainly gypsum) are formed on the surface of the carbonaceous materials. After years of exposure, this crust is able to trap and accumulate the previously mentioned pollutants due to its porous nature. The inclusion of carbonaceous and other metallic particles gives the characteristic colour to this crust [6].

Even if there are many protocols to conduct decontamination of metals from construction materials [7,8], there is not a standardized analytical methodology to detect this contamination in the material itself or in the formed crusts. Considering the ability of this patina to accumulate organic and metallic contaminants, its contribution can be considered harmful not only for the users of the construction, but also for the workers that can repair, renovate, restore or conduct demolition works of the building. Researchers/specialists that can undertake sampling procedures for a subsequent study of the materials are also a segment potentially exposed to these pollutants.

To evaluate the hazardousness of black crusts growing on construction materials in terms of metallic contamination, it should be necessary to evaluate the nature of the accumulated metals and their concentrations in the BCs. Moreover, an imaging study will allow to determine if those metals are distributed on the surface (recent depositions) or if they are accumulated inner in the BCs (past metallic accumulations). To achieve this objective, a superficial analysis of the BCs would not offer successful results, since it would not allow to obtain the in-depth distribution of the metals in the BCs. For that, the preparation of the sample as a thin section will be required. In the literature, several authors remark the necessity of this specific sample preparation [9-11]. However, most of the works deal with the characterization of the BCs composition and the substrate (construction material) in which they are formed, and they do not go in depth in the identification of the accumulated metals, the evaluation of their distribution in the BCs and the identification of the molecular form (speciation) in which those metals are present.

In this work, we present the development and application of an analytical methodology useful to obtain information about the nature, concentration and distribution of superficial and internal metallic contamination on BCs growing on cement and concrete from Punta Begoña Galleries, a historical construction located in Getxo (Basque Country, Spain). In order to detect quickly and in a cost-effective way the metallic accumulations and their specific position in the BCs, samples were prepared as thin sections and studied using spectroscopic imaging techniques. Scanning Electron Microscopy coupled to Energy Dispersive spectrometry (SEM-EDS) and micro Energy Dispersive X Ray Fluorescence spectrometry (μ-EDXRF) techniques allowed to identify the nature, position and distribution of the metals in the cross-section of the BCs. Once the exact position was defined, Raman imaging was used to perform the speciation analysis in order to identify which ones are the main molecular forms of the metals accumulated in the studied BCs. The obtained experimental evidences were used to propose the reactivity pathway of the detected newly formed metallic compounds, whose presence was confirmed by chemical equilibrium modelling. In order to evaluate if the metallic contamination accumulated

in the BCs can be considered hazardous, quantification of metals was also conducted using Inductively Coupled Plasma- Mass Spectrometry (ICP-MS) technique. Finally, to approach the source of emission of the detected Pb accumulations, lead isotopic ratio analysis was also included in the methodology.

2. MATERIALS AND METHODS

2.1. Sampling

BCs specimens were sampled from exposed facades from the Punta Begoña Galleries, a construction from the early 20th century located in Getxo (Basque Country, North of Spain), just in front of the sea [12]. This construction is involved in a recovery and value enhancement project in which decisions about the recovery or remove process of materials will be made [13]. BCs samples were extracted from the oriented northwest Upper (UG) level and oriented southwest Lower (LG) level of the construction. The sampling areas are presented in Fig. 1. Three replicate samples were extracted from each sampling area and analyzed in order to guarantee the representativeness of the results.

2.2. Sample preparation

For the analysis by elemental and molecular spectroscopic imaging techniques, BCs samples were prepared as thin sections following the method used for realizing the petrographic thin sections.

For the analysis by X-Ray Diffraction (XRD) and Inductively Coupled Plasma Mass Spectrometry (ICP-MS), BCs samples were manually grinded in an agate mortar.

2.3. Analytical Techniques and methodology description

The mineralogical characterisation of the BCs samples was achieved grinding the BCs samples and subjecting them to a semi-quantitative estimation of the principal crystalline compounds (above 1 % w/w) by means of XRD using a D2 PHASER diffractometer (Bruker/AXS GmbH, Germany). The X-ray source used was a common sealed X-ray tube with copper anode (30 kV, 10 mA and 300W). Cu Kα radiation (λ= 1.5418 Å) to irradiate the sample was obtained by the use of nickel filter. The instrument allows obtaining continuous scans from 5 to 70° 2θ with a step width of 0.02° and 1 second per step as counting time.

To detect the metallic accumulation in the BCs and its distribution two techniques were used. On the one hand, an EVO LS10 Zeiss Scanning Electron Microscope coupled to a QUANTAX XFlash 6|30 Energy Dispersive Spectrometer (Bruker Microanalysis). The software employed for data acquisition and treatment was the Bruker ESPRIT 1.9.

On the other hand, the M4 TORNADO EDXRF spectrometer (Bruker Nano GmbH, Germany) was also used to map the BCs thin sections. The set-up including the poly-capillary lens was employed to achieve a lateral resolution down to 25 m (measured for Mo K_α). . The spot size varies as a function of the energy, being 17 μm at 2.3 keV and 32 μm at 18.3 keV. To acquire the spectral information, the Rh X-ray tube was programmed at the maximum voltage (50 kV) and current (600 μA). The detection of the fluorescence radiation was performed using an XFlash® silicon drift detector with 30 mm^2 sensitive area and energy resolution of 145 eV for Mn-K_α energy. In order to improve the detection of the lightest elements (Z<19) measurements were acquired under vacuum (20 mbar). The spectral data acquisition and treatment was performed using the M4 TORNADO software. Prior to obtain the Hyper Maps presented in this work, the elemental assignation and deconvolution was conducted in order to minimize the possible spectral interferences and to reject the presence of artefacts. The elemental maps were obtained according to the intensity of K_α line of each element detected. Further details of this instrument can be found elsewhere [14].

The quantification of the main metals accumulated in the BCs samples and their respective construction materials was conducted using a NexION 300 ICP-MS (Perkin Elmer, Ontario, Canada) working in a class 100 clean room. For the metals extraction, 0.5 g of BCs and construction materials were accurately weighed and subjected to an acid extraction in a microwave oven using 3:1 HNO_3 (69%)-HCl (36%) following the EPA 3051A method [15]. In the lead isotopic analysis, dead time and mass discrimination corrections were performed in order to obtain accurate lead isotope ratios. The procedure and equations to be applied can be found in F. Vanhaecke et al. 2008 [16]. Linear model was used for the calculation of the mass bias factor using $^{203}Tl/^{205}Tl$ ratio from a 10 ng·g^{-1} Tl solution continuously added and mixed with the sample via a T piece. Finally, the data treatment was performed with the Elan 3.2 software (Perkin Elmer SCIEXTM, Ontario, Canada).

To identify the main molecular phases including the detected metals in the BCs, the inVia confocal Raman microscope (Renishaw, Gloucestershire, UK) was used following both, a single point and mapping analysis strategy. The spectrometer is coupled to a DMLM Leica microscope, which can use a great variety of long-range lens (5x, 20x, 50x and 100x). For the spectral acquisitions, in order to minimise fluorescence effect, the 785 nm NIR excitation laser was used.

The laser power (output power) at the source is 350 mW, and about 150 mW (set as 100% of the laser power) at the surface of the analysed sample. In order to reduce the acquisition time, the Raman image acquisitions were performed using the StreamLine^{TM} Plus option, which is able to generate chemical images preventing laser induced sample damage by illuminating with a line of laser light, rather than an intense spot. Once the spectra of the selected area under study were obtained, a spectral treatment consisted of filtering and baseline correction was applied. Finally, in order to represent the distribution maps, the regions/bands of the components of interest were selected, thus an individual distribution map for each of them was obtained based on the relative intensity of that band in each measurement point (represented as a pixel in the image). The Raman distribution images were acquired using the Wire 3.0 software (Renishaw, UK).

In order to thermodynamically confirm the existence of experimentally detected molecular compounds by Raman microscopy, chemical equilibrium modelling was conducted using the MEDUSA software [17] and extracting specific constants from Visual MINTEQ software [18]. The components and their total concentrations to include in the software were taken from experimental results obtained during the characterisation of the samples.

3. RESULTS AND DISCUSSION

3.1 Classification of BCs samples according to their mineralogy

In Table 1, the mineralogical composition of the BCs under study is displayed together with a description of the sampling area and the colour/morphology of the samples (see Fig. S-1 from Supplementary Material section).

The main component, as expected, is gypsum ($CaSO_4 \cdot 2H_2O$) [19]. However, there are also significant differences in the gypsum content (ranging from 65 to 97%) depending on the considered sample. The BCER sample taken from the concrete external railing of the construction is the most common BCs, since it is mainly composed of gypsum together with some quartz (α-SiO_2) elements/clasts coming from soil dust depositions, probably sand of the nearby beach [20]. These BCs type are totally exposed to the atmosphere without any protection, except the one provided by the railing itself. BCLG-3 sample presents lower gypsum content, apart from quartz, calcite ($CaCO_3$) and some potassium aluminosilicates presence.

The BCLG-1 and BCLG-2 samples, collected on the wall of the Lower Gallery, showed a characteristic orange colour (see Fig. S-1 from Supplementary Material), which can be related with jarosite ($KFe_3(OH)_6(SO_4)_2$) presence, identified by XRD as one of the majors compounds of these samples. In the walls where these samples were taken (see Fig. 1), a red coloration coming from the iron leaching of the reinforcement of the concrete of the ceiling is observable. The solubilised sulphate ions coming from the BCs matrix can react with the leached iron to form jarosite in these specific BCs.

In Fig. S-2 from Supplementary Material, a SEM image of the representative gypsum and jarosite crystals composing the BCs matrix of BCLG-1 and BCLG-2 samples can be observed (see Fe and S presence detected by EDS in crystals S-1 and S-3 from Fig.S-2). The combined detection of Si, Al and K in the crystals from these BCs by EDS agrees with the identification of illite by XRD (see Fig.S-2 from Supplementary Material).

3.2 Identification of metallic accumulations in the BCs prepared as thin sections using elemental imaging spectroscopic techniques

The replicate BCs samples from each location prepared as thin sections were analyzed using SEM-EDS and μ- EDXRF techniques in order to detect metallic particles trapped on them. Using SEM-EDS, it was possible to assess that those particles are mainly composed of Fe. Moreover, aluminosilicate and quartz elements were also observable probably coming from the deposition of the beach sand in front of the construction.

Depending on the analysed BCs, the abundance of these particles was different. BCLG-1 and BCLG-2 were the ones presenting a lower particulate matter (PM) presence. This could be due to the orientation of the BCs in the construction. The highest PM depositions were observed in BCUG-3 (see Fig. 2 and Fig. S-1 from Supplementary Material) and BCUG-1 and 2 (see Fig. 1). The analyses of some of the particles contained in these BCs showed the presence of Ti, Cr, Mn, Cu and Zn together with Fe.

The observations conducted by SEM on BCUG-2 thin section, allowed to detect a very bright area in the BCs part closer to the mortar of the wall (see Fig. 3A and B), showing the main presence of lead (see spectrum S-1 in Fig. 3). This metal accumulation was observed in all the BCs collected in the Upper Gallery (BCER, BCUG-1, BCUG-2, BCUG-3), which are the ones more exposed to the atmosphere. The Pb accumulation is located in the BC area in contact with their corresponding mortars (BCUG-1 to 3) or concrete (BCER), in contrast to Fe, identified as deposited particles in the middle/outer parts of the BCs (see Fig. 3A and spectrum S-2). As Pb

was not detected in the outer-middle of the BCs, it can be affirmed that it was mainly deposited in the past and retained at the beginning of the BCs formation. The experimental observations lead us to conclude that in the outer-middle parts of the BCs, Pb is not present or its concentration is lower than the detectable one by EDS or μ- EDXRF.

The highest lead accumulation area was observed in BCER, since it can reach up to around 1.5 mm x 400 mm in the thin section, thus it is visible at the naked eye (see Fig. 4A). This lead bright area was mapped by means of SEM-EDS detecting the presence of Na, Mg, Al, Si, S, Cl, K, Ca, Fe, Zn and Pb (see Fig. 4B). The distribution map of Pb suggests that this metal is related with Cl, S and Zn (see Fig. 4C-E). On the contrary, Fe is present as hot spots in the EDS image (see Fig. 4H). In order to verify if a correlation between Pb and S exists, a deconvolution of the S-K_α and Pb-M_α should be conducted due to the high interference between some of their respective spectral lines (S K_α and Pb L_α). To verify this hypothesis and thanks to the big area covered by Pb in BCER sample, it was decided to perform a μ- EDXRF imaging analysis of this same area.

In the Fig.5, an example of a μ- EDXRF mapping from a thin section of BCER is shown. The mapped area was 20.604 x 7.992 mm and the step size used for the spectra acquisition was 20 μm. Each spectrum inside the mapped area was acquired during 50 ms and 2 cycles were run to obtain the final mapping result. As it can be observed in the sum spectrum shown in Fig. 5B, representative of the whole mapped area, elements such as Na, Mg, Al, Si, S, Cl, K, Ca, Ti, Cr, Mn, Fe, Cu, Zn, Sr, Zr, Ba and Pb were detected. Elements with Z<13 are not show in this last image to simplify the visualization. In this case, it was possible to detect elements such as Ti, Cr, Mn, Cu, Sr, Zr and Ba, not detected by SEM-EDS. In Fig. 5C-H, an example of the distribution maps for some of the detected elements is shown. Ca and S distribution maps represent the gypsum presence in the BCs (see Fig. 5C). It can also be appreciated some blue areas belonging probably to calcite fragments. Moreover, Fe is highly distributed in the external and internal parts of the BCs (See Fig. 5D), agreeing with the detection of a wide variety of Fe particles by SEM-EDS.

Elements such as Cr and Zr are scarcely distributed in the BCs. Ti, Ba and Mn are present in the thin section as hot spots in the external and internal parts (see Fig. 5E and F), while Zn and Cu show a coincident distribution in the internal parts of the BCs (see Fig. 5D). Notice that Cu also shows some accumulation points in areas where Zn is not present (see blue areas in Fig. 5D). This observation suggests that, as it happens with Pb, these two last metals were accumulated in the initial steps of the BCs formation and they remained encapsulated in the inner parts of the BCs.

The joint distribution of Pb and Cl, firstly observed in the SEM-EDS analysis (see Fig.4C and D), was confirmed with the μ- EDXRF imaging (see Fig. 5G). In order to determine if Pb and S are correlated in the BCER, the S K_α-Pb L_α distribution map was obtained after the corresponding deconvolution of S-K_α and Pb-M_α lines (see Fig. 5H). Considering that in the area of high Pb accumulation S is not present, it is demonstrated that the S distribution obtained in the SEM-EDS analysis was due to the Pb-M_α line and not to the S K_α.

3.3. Determination of iron, lead, zinc and copper maximum concentrations on the BCs

Three replicate samples from BCER were subjected to acid extraction and to a subsequent quantification by ICP-MS of the highly accumulated metals (Fe, Pb, Zn and Cu), in order to determine the maximum levels of them inside the BCs. BCER was selected as the most impacted sample in order to have the maximum accumulation values on the BCs from the construction. Apart from the patina, the concrete adhered to the BCs was also subjected to the same procedure.

Considering that Fe particles are being accumulated not only in the internal parts of the BCER but also in the outer areas, the concentration of this element is the highest one, reaching values up to 3% in weight (% w/w). The concentrations of Cu, Zn and Pb in the concrete were set below 50 mg·kg^{-1}. On the contrary, in the BCER the detected concentrations were 153 ± 11, 568 ± 45 and 3350 ± 70 mg·kg^{-1} respectively. Pb concentration in concretes and cements usually never exceed 300 mg·kg^{-1} [21], thus the concentration values determined in the concrete close to the BCER cannot be considered a source of Pb for the BCER. The concentration of lead in this BC can be considered very high and could contribute to include additional metallic contamination to the construction material/BCs ensemble.

3.4. Speciation study of the main metals accumulated in the BCs by means of Raman imaging

The Pb, Zn and Cu accumulation areas in BCER thin section shown in Fig.5 were exhaustively analysed following a single point and imaging strategy by Raman microscopy in order to identify the main molecular forms of these metals. Regarding the identification of the mineralogical phases of Zn and Cu, it was not possible to detect any Raman signal. On the contrary, Raman signals related with lead compounds were easily detected. As the Pb concentration is much

higher (22 and 6 times higher than the one of Cu and Zn respectively), it could be reasonable not being able to detect experimentally their molecular forms by Raman microscopy.

Two main lead compounds were detected in the Pb accumulation area, laurionite (PbClOH), with bands at 124, 269 and 327 cm^{-1}, and hydrocerussite ($Pb_3(CO_3)_2(OH)_2$), showing its main band at 1051 cm^{-1} (see Fig. 6 A) [22,23]. The molecular results confirm that previously detected Cl-Pb elemental joint distribution can be related with the presence of laurionite. Apart from the mentioned Pb compounds, a band at 971 cm^{-1} which can be attributed to the ν_1 of PO_4^{3-} was also detected [24]. A possible compound related with it can be tsumebite, $Pb_2Cu(PO_4)(SO_4)(OH)$, which presents its principal band at 971 cm^{-1} [25]. Considering that this Raman band was detected in few isolated spectra acquired by single point analysis and it was not possible to detect its presence by Raman imaging, this kind of phosphate can be present at very low concentrations.

In Fig.6B-D, the distribution maps of laurionite (spectral range 123-156 cm^{-1}), hydrocerussite (spectral range 1042-1059 cm^{-1}) and calcite (spectral range 1080-1090 cm^{-1}) are shown. Laurionite is mainly distributed in the Pb accumulation area, while hydrocerussite is sporadically present (as hot spots) and close to the calcite presence. Probably, this lead carbonate was formed owing to the reaction of laurionite with solubilised calcium bicarbonate coming from the calcite layer close to laurionite.

3.5. Proposal of the reactivity pathway leading to the formation of lead compounds and its confirmation using chemical equilibrium modelling

The elemental and molecular experimental results suggest that the lead compounds accumulated in the BCs can come from lead particle emissions that took place close to the construction in the past. This metal can be emitted by industries to the atmosphere as airborne particulate matter, which can suffer a subsequent oxidation (PbO formation) [26]. Considering that the construction is placed just in front of the sea, the chloride input is guaranteed. Therefore, the PbO can react with the chlorides from the marine aerosol to form laurionite (see reaction 1). Additionally, PbO can react with the atmospheric CO_2 to form hydrocerussite (see reaction 2) [22]:

$2 PbO + H_2O + 2 Cl^- \rightarrow 2 PbClOH$ (1)

$3 PbO + H_2O + 2 CO_2 \rightarrow Pb_3(CO_3)2(OH)_2$ (2)

In order to confirm the formation and possible co-existence of these compounds, chemical equilibrium modelling was run with MEDUSA software. The precipitation constant of hydrocerussite was extracted from the Visual MINTEQ software database.

Before constructing the chemical equilibrium modelling, it is necessary to consider that the starting point to explain the laurionite and hydrocerussite formation is a diluted solution which contains lead with other ions (chlorides and carbonates) necessary for their formation, that wets the surface of the BCs. This solution should be gradually concentrated while its water evaporates. This concentration process will promote the saturation of one or more mineral phases, which precipitate (laurionite and hydrocerussite in this case). Considering that, an evaporation process will always took place, high concentrations of lead and the other anions should be consider in the chemical equilibrium modelling other than the experimentally determined ones in section 3.3.

In Figs. 7A-D, some mole fraction diagrams showing the predominant stable components in mass fraction depending on the pH are shown. Different concentrations of Pb in the presence of 1.00 mM of CO_3^{2-} (average concentration of CO_2 values in the atmosphere of the 20th century) were tested in order to corroborate the stability of hydrocerussite. The predominance of hydrocerussite at more acidic pH, closer to the pH of the acid rainwater (5- 5.5) in the vicinity of the construction is higher when Pb concentration is increased in comparison to the carbonate (see Figs. 7A-D). At lower concentrations of lead, $PbCO_3$ becomes important. This observation reinforces the necessity of having high Pb concentrations for the formation of hydrocerussite.

To confirm the formation of laurionite and the possible combined presence of this lead compound and hydrocerussite, Cl was added to the system (see Figs. 7E-H). Although at 10 mM of Pb, the laurionite presence is high, (see Fig. 7F), if the concentration of Cl^- and Pb is increased (see Figs. 7G and H), the predominance of laurionite is complete. At 10 mM of Pb the presence of hydrocerussite is very low at the pH of the rainwater, and when Cl^- and Pb concentrations increase even more, it disappears completely (see Figs. 7H). These high Pb and Cl concentrations could be reached when wet aerosol is evaporated nearly to completion. Notice that to explain the formation of laurionite, the concentration of chlorides in solution must be higher than the one of lead, which is guaranteed in this location.

3.6. Lead isotopic analysis to identify the possible source of lead emissions

In order to determine the possible emission source of Pb, lead isotopic analysis was conducted on the BCER and the concrete next to it. The ^{206}Pb/^{207}Pb ratios obtained were 1.190 ± 0.002 and 1.177 ± 0.003, and the ^{208}Pb/^{206}Pb ratios 2.073 ± 0.005 and 2.082 ± 0.005 for the concrete and BCs respectively. These values are inside the established range (1.16 and 1.21) for lead contained in coal in Europe [27], which agrees with lead isotope ratios in Spanish coals determined in a work by Díaz-Somoano et al. [28]. In particular, the ^{206}Pb/^{207}Pb ratios ranged between 1.16-1.20, and ^{208}Pb/^{206}Pb ratios between 2.00-2.10 for the coal coming from the Central Asturian Coal Basin [28], values which are very close to the ones determined in this study. The ^{206}Pb/^{207}Pb ratio found for the lead contained in old gasolines is lower, around 1.12 or smaller [29]. Thus, according to the values obtained in this work, the presence of lead coming from old gasolines is discarded.

Considering this information, it is highly possible that the lower concentrations of Pb found in the mortar samples with a ^{206}Pb/^{207}Pb ratio of 1.19 belong to geogenic lead [27], while the decrease in the ^{206}Pb/^{207}Pb ratio from 1.190 in the concrete to 1.177 in the BCER could be related to coal burning. In fact, when coal is burned, lead particles can be emitted to the atmosphere and they can suffer a subsequent oxidation and deposition process on the materials. This is a quite plausible theory due to the location of Punta Begoña Galleries close to an old power station plant, which worked with carbon since the 60´s, with continuous coal loadings and unloadings. The presence of higher Pb accumulation in the inner parts of the BCs makes also sense, since coal combustion was much higher in the past than nowadays.

4. CONCLUSIONS

The analytical methodology proposed in this work allowed to conclude that BCs can be used not only as passive samplers of atmospheric metal pollution, but also as a source of information of past and recent heavy metals emissions to the atmosphere, providing in this sense a comprehensive knowledge about the atmospheric metal pollution of the surrounding environment.

The combined use of elemental and molecular imaging techniques demonstrated that a superficial screening of the BCs could offer incomplete results regarding metallic contamination on BCs. In this specific case study, the accumulated Cu, Zn and specially Pb remained hidden during the superficial SEM-EDS analysis and bring to conclude that the main metal present in the BCs was Fe. Moreover, if only a destruction of the BCs and a subsequent quantification of the metals would be performed, it would not be possible to determine if this metal was

concentrated in the surface or in the inner areas of the BCs. Thus, it is highly recommendable to prepare BCs as thin sections and to perform a depth profile study by means of imaging techniques. Moreover, considering that μ- EDXRF usually improves the limit of detection of heavier elements (Z>26), when the area of the metallic accumulation is in the order of some mm^2, it is recommendable to use μ- EDXRF technique instead of SEM-EDS. If these techniques are not able to detect the presence of metals (limits of detection/quantification of some mg/kg), it can be concluded that the concentrations of possible metals present in the BCs are too low in order to consider this kind of crusts as potentially hazardous materials for the environment and for human health.

In this specific case study, the speciation analysis carried out by Raman imaging allowed to conclude that the concentration of lead particles emitted in the past to must have been high to promote the formation of the identified lead compounds. Moreover, the role of the direct influence of the marine atmosphere in the formation of the identified lead compounds have been clearly proven.

The acid destruction of the BCs allowed also determining the concentration of the main metals accumulated in the whole mass of the patinas. This information would be useful to evaluate the acid extractable concentration of the metals present in the BCs. However, in order to approach the potential "leachable toxic" characteristic of the BCs, it could be more suitable to apply a less aggressive treatment such as an extraction procedure using acetic acid or EDTA^{2-}. Although in this case a more aggressive extraction procedure was applied, the obtained concentration of lead in the BCs (higher than 0.3 % w/w) can be considered sufficiently high to suggest these patinas as possible source of metallic contamination.

Considering that these kind of crust can be a source of metallic contamination, if research studies which involve the removal of these crusts or if restoration processes in the construction should be conducted, appropriate individual protections should be used. In the most extreme case, when any construction material having such BCs must be removed from the building for its recycling or its management as waste product, it would be recommendable to remove this patina carefully in order to extract the metallic contamination from the BCs/construction material ensemble.

Acknowledgements

REFERENCES

1. Ozga I, Ghedini N, Bonazza A, Morselli L, Sabbioni C. The importance of atmospheric particle monitoring in the protection of cultural heritage, WIT Trans. Ecol. Environ. 2009;123:259–269.

2. Valotto G, Zannoni D, Rampazzo G, Visin F, Formenton G, Gasparello A. Characterization and preliminary risk assessment of road dust collected in Venice airport (Italy). J. Geochem. Explor. 2018;190:142–153.

3. Bonazza A, Sabbioni C, Ghedini N. Quantitative data on carbon fractions in interpretation of black crusts and soiling on European built heritage. Atmos. Environ. 2005;39(14):2607–2618.

4. Gaviño M, Hermosín B, Vergès-Belmin V, Nowik W, Sáiz-Jiménez C. Composition of the black crusts from the Saint Denis Basilica, France, as revealed by gas chromatography-mass spectrometry. J. Sep. Scien. 2004;27(7-8):513-523.

5. Hermosin B, Gaviño M, Saiz-Jimenez C. Organic compounds in black crusts from different European monuments: a comparative study, in: C. Saiz-Jimenez (Eds.), Air Pollution and Cultural Heritage, CRC Press, Florida, 2004, pp. 47-55.

6. Morillas H, Maguregui M, García-Florentino C, Carrero J.A, Salcedo I, Madariaga J.M. The cauliflower-like black crusts on sandstones: A natural passive sampler to evaluate the surrounding environmental pollution. Environ. Res. 2016;147:218-232.

7. Yurchenko A.Y, Karlin Y.V, Nikolaev A.N, Karlina O.K, Barinova A.S. Decontamination of radioactive concrete. Atom. Energy. 2009;106:225-230.

8. Kim G.N, Choi W.K, Lee K.W. Decontamination of radioactive concrete using electrokinetic technology. J. Ap. Electrochem. 2010;40(6):1209-1216.

9. Ruffolo A.A, Comite V, La Russa M.F, Belfiore C.M, Barca D, Bonazza A, Crisci G.M, Pezzino A, Sabbioni C. An analysis of the black crusts from the Seville Cathedral: A challenge to deepen the understanding of the relationships among microstructure, microchemical features and pollution sources. Sci.Tot. Environ. 2015;502:157-166.

10. Pozo-Antonio J.S, Pereira M.F.C, Rocha C.S.A. Microscopic characterisation of black crusts on different substrates. Sci. Tot. Environ. 2017;584-585:291-306.

11. La Russa M.F, Fermo P, Comite V, Belfiore C.M, Barca D, Cerioni A, De Santis M, Barbagallo L.F, Ricca M, Ruffolo S.A. The Oceanus statue of the Fontana di Trevi (Rome): The analysis of

black crust as a tool to investigate the urban air pollution and its impact on the stone degradation. Sci. Tot. Environ. 2017;593-594:297-309.

12. García-Florentino C, Maguregui M, Morillas H, Balziskueta U, Azcarate A, Arana G, Madariaga J.M. Portable and Raman imaging usefulness to detect decaying on mortars from Punta Begoña Galleries (Getxo, North of Spain), J. Raman Spectrosc. 2016;47(12):1458-1466.

13. http://puntabegonagetxo.eus/ [last accessed 2018 October 26]

14. García-Florentino C, Maguregui M, Romera-Fernández M, Queralt I, Margui E, Madariaga J.M. Usefulness of a Dual Macro-and Micro-Energy Dispersive X-ray Fluorescence Spectrometer to Develop Quantitative Methodologies for Historic Mortar and Related Materials Characterization. Anal. Chem. 2018;90(9):5795-5802.

15. EPA Method 3051A, 2007, Microwave assited Acid Digestion of Sediments, sludges, soils and oils, (n.d.).

16. Vanhaecke F, Balcaen L, Taylor P. Inductively coupled plasma spectrometry and its applications. 2008. Ed. Steve J. Hill. Pag 172-177.

17. Puigdomenech I. MEDUSA (Make Equilibrium Diagrams Using Sophisticated Algorithms), Dep. Inorg. Chem. R. Inst. Technol. KTH Stockh. Swed. (2009).

18. Gustafsson J.P, MINTEQ, R. Inst. Technol. KTH Stockh. Swed. (2013).

19. Fronteau G, Schneider-Thomachot C, Chopin E, Barbin V, Mouze D, Pascal A. Black-crust growth and interaction with underlying limestone microfacies. Geol. Soc. Lond. Spec. Publ. 2010;333:25–34.

20. Calparsoro E, Maguregui M, Giakoumaki A, Morillas H, Madariaga J.M. Evaluation of black crust formation and soiling process on historical buildings from the Bilbao metropolitan area (north of Spain) using SEM-EDS and Raman microscopy. Environ. Sci. Pollut. Res. 2017;24(10):9468–9480.

21. Dobidzewska M. Waste materials used in making mortar and concrete, J. Mat. Educ. 39 (2017) 133-156.

22. Frost R.L, Williams P.A. Raman spectroscopy of some basic chloride containing minerals of lead and copper. Spectrochim. Acta. A. Mol. Biomol. Spectrosc. 2004;60(8-9):2071–2077.

23. Frost R.L, Martens W, Kloprogge J.T, Ding Z. Raman spectroscopy of selected lead minerals of environmental significance. Spectrochim. Acta. A. Mol. Biomol. Spectrosc. 2003;59(12):2705–2711.

24. Ranjkesh B, Chevallier J, Salehi H, Cuisinier F, Isidor F, Løvschall H. Apatite precipitation on a novel fast-setting calcium silicate cement containing fluoride. Acta Biomater. Odontol. Scand. 2016;2(1)68–78.

25. Downs R.T, Hall-Wallace M. A Database of Crystal Structures. Published in the American Mineralogist and the Canadian Mineralogist and Its Use as a Resource in the Classroom, 18th Gen. Meet. Int. Mineral. Assoc. (2002).

26. Ettler V, Johan Z, Beronnet A, Jankovsky F, Gilles C, Mihaljevic M, Sebek O, Strnad L, Bezdicka P. Mineralogy of air-pollution-control residues from a secondary lead smelter: environmental implications. Environ. Sci. Technol. 2005;39(23):9309-9316.

27. Komárek M, Ettler V, Chrastný V, Mihaljevič M. Lead isotopes in environmental sciences: A review. Environ. Int. 2008;34(4):562–577.

28. Díaz-Somoano M, Suárez-Ruiz I, Alonso J.I.G, Ruiz Encinar J, López-Antón M.A, Martínez-Tarazona M.R. Lead isotope ratios in Spanish coals of different characteristics and origin. Int. J. Coal Geol. 2007;71:28–36.

29. Monna F, Poujol M, Losno R, Dominik J, Annegarn H, Coetzee H. Origin of atmospheric lead in Johannesburg, South Africa. Atmos. Environ. 2006;40(34):6554–6566.

Figure 2. Microscopic observations of BCUG-3 thin section under the SEM showing the particles trapped at different magnifications together with the EDS spectra of two specific Fe particles (S-1 and S-2).
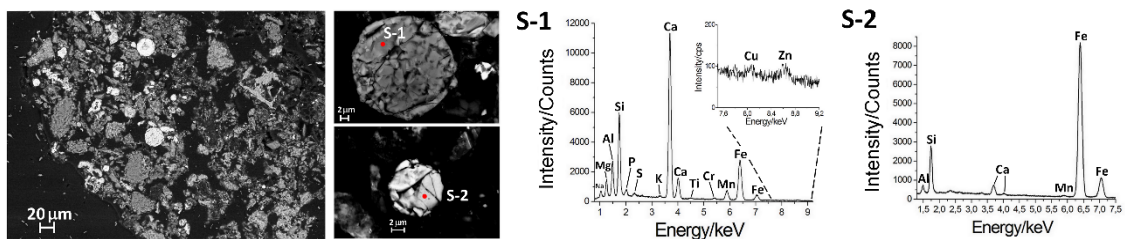
Figure 3. A) SEM image of BCUG-3 thin section showing the metallic accumulations (S-1) close to the mortar and trapped particles (S-2), B) A magnification of the metallic accumulations on BCUG-3 thin section. At the right of the image, the representative spectra of S-1 and S-2 in Figure A are shown.
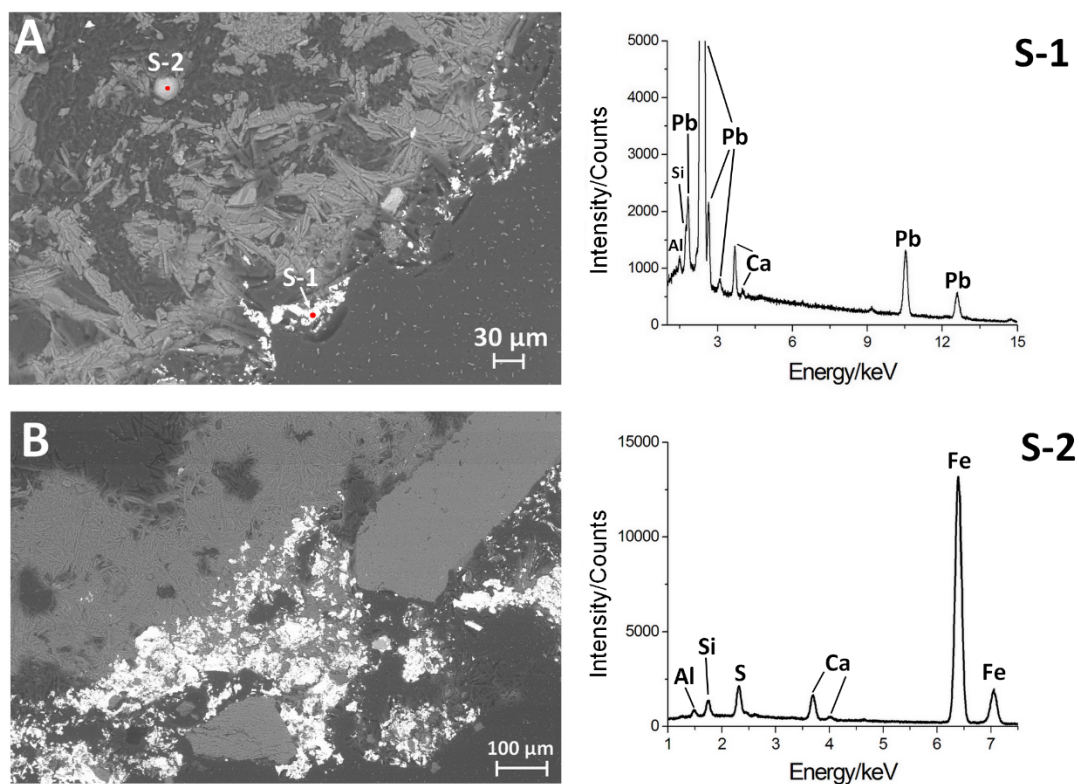
Figure 4. A) Area mapped by EDS of BCER thin section, B) Sum spectrum of the analysed area divided in two sections (lighter elements on the left and heaviest elements on the right), C) Pb distribution map, D) Cl distribution map, E) S distribution map, (F) Zn distribution map, G) Ca distribution map, H) Fe distribution map.
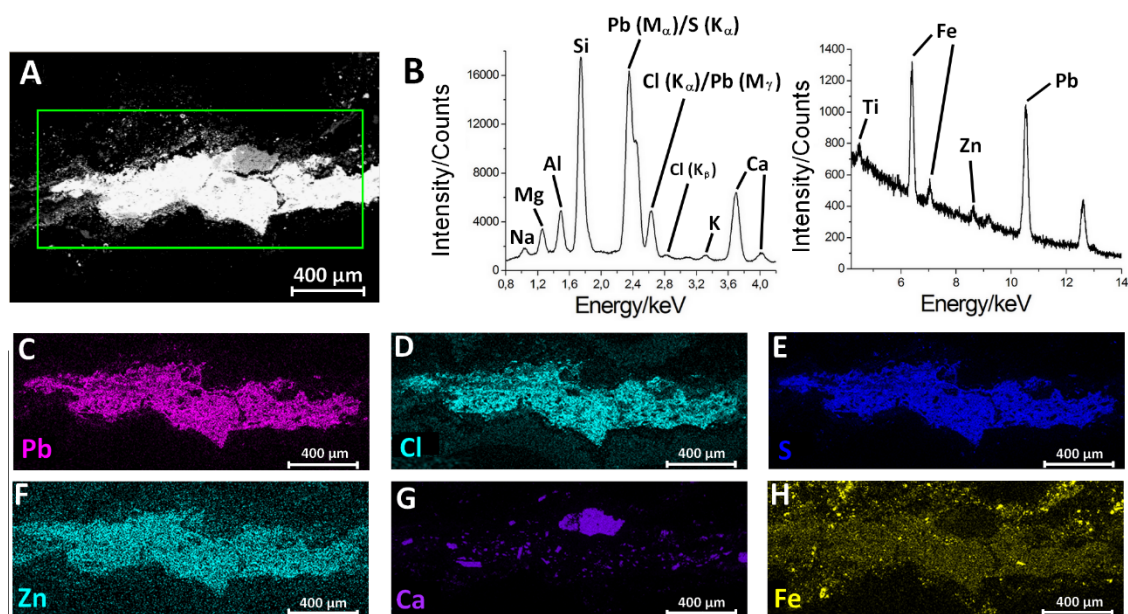
Figure 5. (A) Visual image of one of the BCER thin section mapped by μ-ED-XRF (B) Sum ED-XRF spectrum of the analysed area in the thin section (C) S and Ca distribution maps (D) Fe, Pb, Zn and Cu distribution maps (E) Ti and Mn distribution maps (F) Ti and Ba distribution maps (G) Pb and Cl distribution maps (H) S and Pb distribution maps.
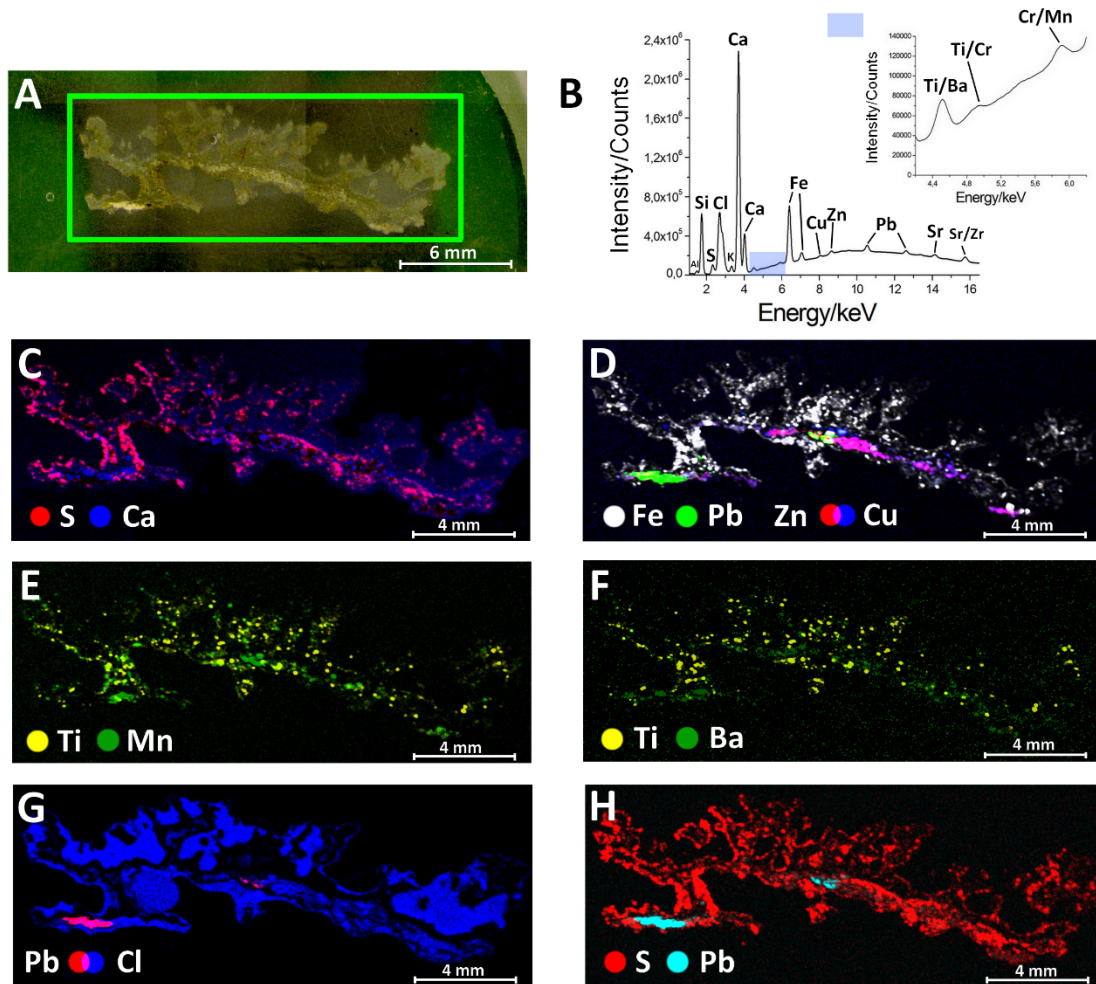
Figure 6. A) Raman spectra acquired on the lead accumulation area from BCER thin section showing the bands of (a) hydrocerussite (b) laurionite (c) laurionite and hydrocerussite (d) laurionite, hydrocerussite and gypsum (e) laurionite, hydrocerussite and PO_4^{3-} at 971 cm^{-1}, (B) Distribution map of laurionite, (C) Distribution map of hydrocerussite (D) Distribution map of calcite.
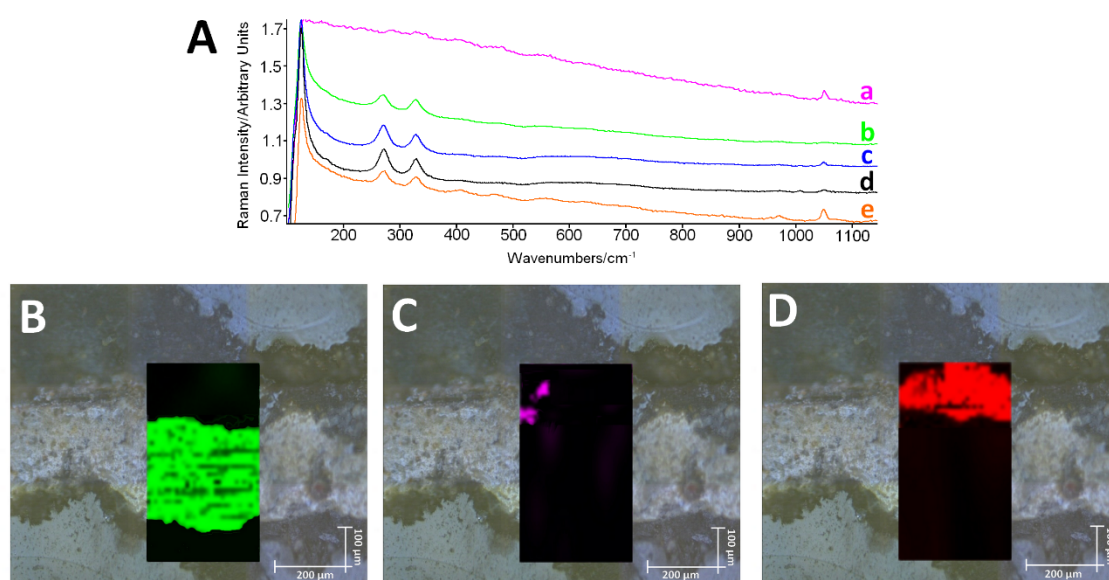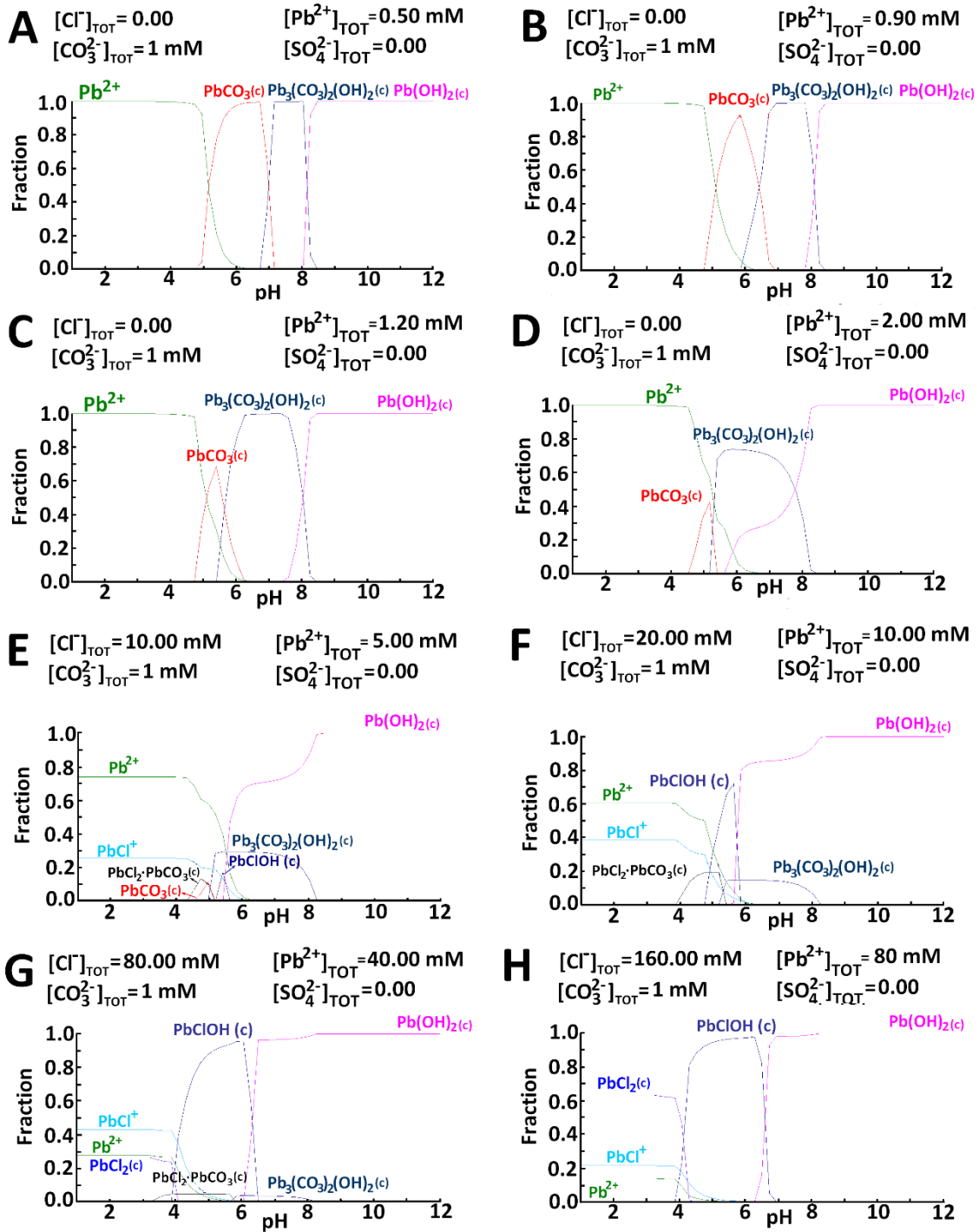
Figure 7. (A-D) Mole fraction diagrams for hydrocerussite depending on lead concentration (E-H) Mole fraction diagrams for laurionite and hydrocerussite depending on chlorine and lead concentrations.

FIGURES SUPPLEMENTARY MATERIAL SECTION

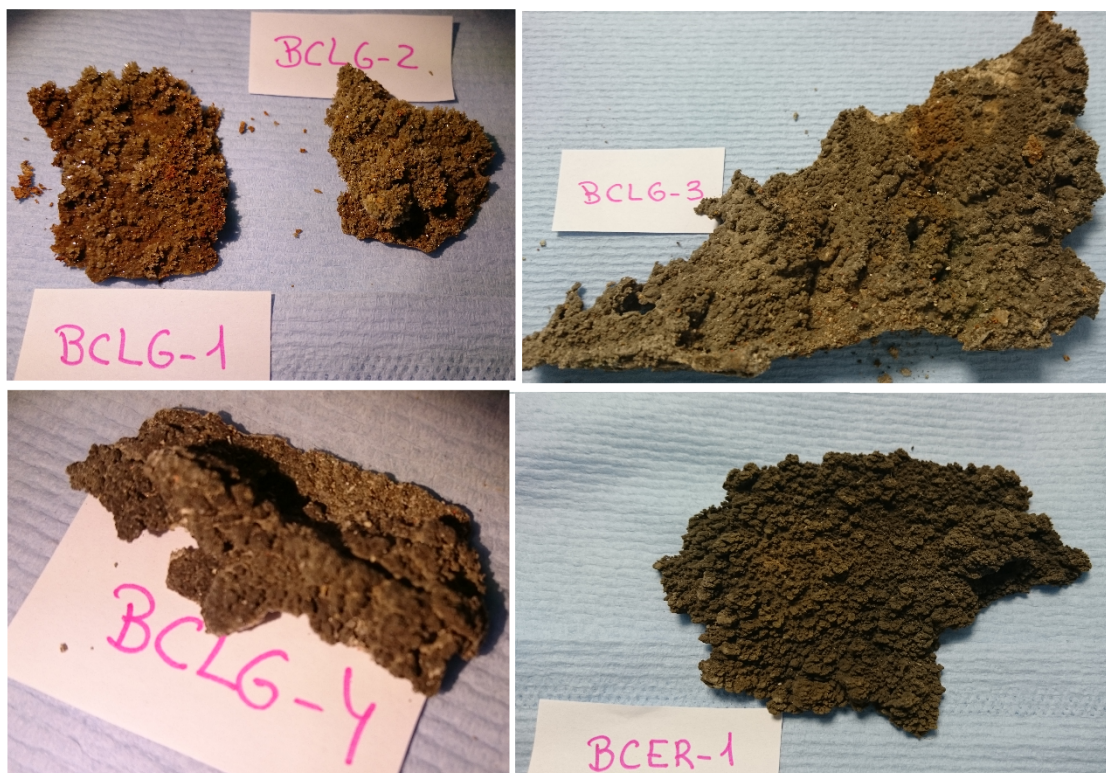**Figure S-1.** Aesthetical appearance of some of the black crust samples.

Figure S-2. SEM microphotograph of the analysed crystal of BCLG-2 and elemental analyses by EDS of the marked points in the crystals.
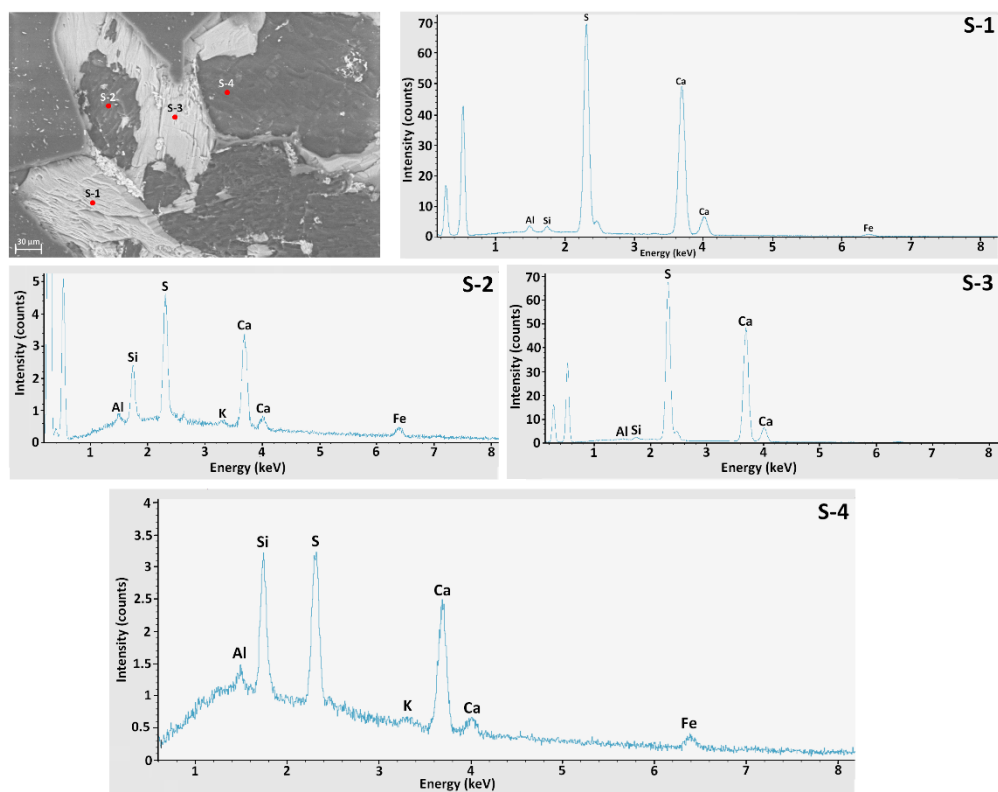
Figure S-3. Lead accumulation areas in the BCER thin section.